arXiv:1503.01006v1 [cond-mat.mtrl-sci] 3 Mar 2015

Two different topological insulator phases in NaBaBi

Yan Sun[1], Qing-Ze Wang[3], Shu-Chun Wu[1], Claudia Felser[1], Chao-Xing Liu[3], and Binghai Yan[1,2*]
[1] *Max Planck Institute for Chemical Physics of Solids, 01187 Dresden, Germany*
[2] *Max Planck Institute for the Physics of Complex Systems, 01187 Dresden,Germany and*
[3] *Department of Physics, The Pennsylvania State University, University Park, Pennsylvania 16802-6300*
(Dated: April 29, 2016)

By breaking the inversion symmetry of the three-dimensional Dirac metal Na_3Bi, we realize topological insulator (TI) phases in the known compound NaBaBi using *ab initio* calculations. Two distinct TI phases emerge: one phase is due to band inversion between the Bi p and Na s bands, and the other phase (under pressure) is induced by inversion of the Bi p and Ba d bands. Both phases exhibit Dirac-cone-type surface states, but they have opposite spin textures. In the upper cone, a left-handed spin texture exists for the s-p inverted phase (similar to a common TI, e.g., Bi_2Se_3), whereas a right-handed spin texture appears for the p-d inverted phase. NaBaBi presents a prototype model of a TI that exhibits different spin textures in the same material. In addition, NaBaBi may exhibit the introduction of correlation effects to the topological state owing to the existence of d states in the band inversion.

PACS numbers: 73.20.At, 71.20.-b, 71.70.Ej

I. INTRODUCTION

In recent years, topological insulators (TIs) have attracted considerable attention owing to their novel fundamental physics and potential applications.[1,2] Because of the nontrivial topology of the bulk band structure, TIs exhibit gapless surface states inside the bulk energy gap. The spin direction is locked to the momentum by spin–orbit coupling (SOC). Thus, the topological surface state (TSS) exhibits a helical spin texture in momentum space. To date, left-handed spin texture is commonly found in known TI materials such as the Bi_2Se_3 family[3–7] and other materials,[8–10] whereas right-handed spin texture has been reported only in HgS.[11]

Topological Dirac semimetals were discovered recently in Na_3Bi [9,12] and Cd_3As_2.[13–17] They also exhibit nontrivial topology in the band structure and can be driven into other exotic topological phases, such as TIs and Weyl metals.[18] For example, the three-dimensional (3D) Dirac point can become massive by breaking a certain crystal symmetry, inducing a TI phase. Following this paradigm, we report a TI material, NaBaBi, synthesized in a recent experiment,[19] which is equivalent to breaking the inversion symmetry of Na_3Bi by replacing two Na sites with one Ba. Furthermore, NaBaBi can be transformed between two different TI phases via external pressure, one with s-p band inversion and left-handed spin texture and the other with p-d band inversion and right-handed spin texture.

II. CRYSTALLOGRAPHIC STRUCTURE AND CALCULATION METHODS

NaBaBi was first synthesized via direct reaction of the elements Na, Ba, and Bi at high temperature in 2004.[19] As shown in Fig. 1(a), NaBaBi exhibits a hexagonal crystal lattice in the $P\bar{6}2m$ space group (No. 189).

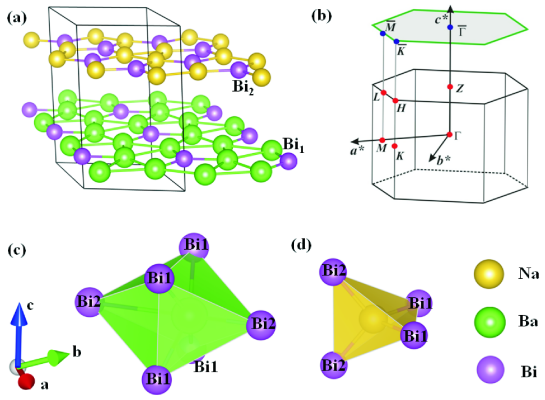

FIG. 1. (color online) (a) Hexagonal crystal lattice for NaBaBi. Two atomic layers, $[(Bi^{3-})_2(Na^+)_3]^{3-}$ and $[(Bi^{3-})(Ba^{2+})_3]^{3+}$, are stacked alternately along the c direction. (b) Corresponding hexagonal Brillouin zone (BZ) and two-dimensional (2D) BZ projected onto the (001) surface. (c), (d) Local environments around Ba and Na atoms are octahedra and tetrahedra, respectively, distorted by Bi atoms.

It is a polar intermetallic compound: two atomic layers are stacked along the c direction in each unit cell, one layer with $[(Bi^{3-})_2(Na^+)_3]^{3-}$ and the other with $[(Bi^{3-})(Ba^{2+})_3]^{3+}$. We can understand the lattice of NaBaBi as a distorted version of that of Na_3Bi. Two equivalent Bi sites that are connected by the inversion symmetry in Na_3Bi become non-equivalent in NaBaBi. The surrounding Ba and Na atoms are in octahedral and tetrahedral environments that are distorted by Bi atoms, as shown in Figs. 1(c) and (d), respectively. In principle, NaBaBi can also be regarded as a low-symmetry version of layered honeycomb ternary compounds, which were recently found to be strong[20] and weak TIs.[21] Be-

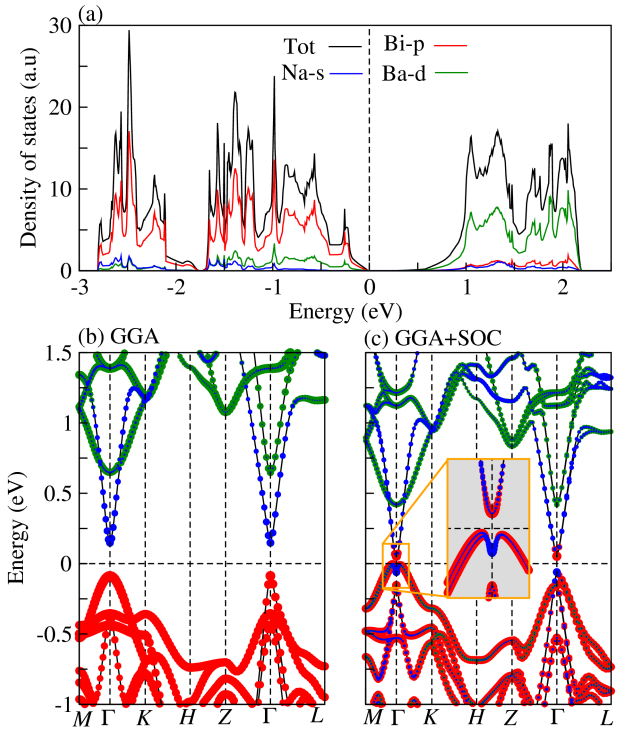

FIG. 2. (color online) Electronic properties of NaBaBi. (a) Total and partial density of states. (b,c) Energy dispersions along high-symmetry lines in lattice momentum space for NaBaBi without and with SOC. Sizes of blue, red, and green dots in (b) and (c) are proportional to the weight contributions of Na s, Bi p, and Ba d orbitals, respectively. Fermi energy has been shifted to zero.

cause the number of total valence electrons is eight in a formula unit, the closed-shell configuration indicates that NaBaBi is possibly an insulator.

To investigate the band structure of NaBaBi, we performed electronic structure calculations using density functional theory (DFT) with the projected augmented wave method,[22] as implemented in the Vienna *ab initio* Simulation Package.[23,24] The exchange-correlation energy was considered in the generalized gradient approximation (GGA) level with the Perdew–Burke–Ernzerhof-based density functional.[25] The energy cutoff is set to 400 eV for the plane wave basis. We adopted k-point grids of $5 \times 5 \times 7$ and $7 \times 7 \times 9$ for the lattice optimization and electronic structure calculations, respectively. The surface band structures are calculated on a slab model in a tight-binding (TB) scheme based on the maximally localized Wannier functions (MLWFs),[26] which are projected from the bulk Bloch wave functions.

III. RESULTS AND DISCUSSION

The band structures in Fig. 2 show that bands near the Fermi energy are contributed by the Bi p, Na s, and Ba d orbitals. Without SOC, NaBaBi is a direct-gap semiconductor with a band gap of 0.23 eV at the Γ point. The highest occupied band is a Bi p_z state, and the lowest unoccupied band is a Na s state, as shown in Fig. 2(b). When the SOC effect is included, the band structure around the Γ point changes dramatically. SOC pushes the Bi p_z band above the Na s band, producing an inverted band structure with an M-shaped valence band [Fig. 2(c)]. Although the Z_2 index cannot be directly calculated from the parity eigenvalues of the Bloch wave functions[27] owing to the inversion asymmetry, the SOC-induced band inversion clearly exhibits a topological phase transition from a trivial insulator to a TI.

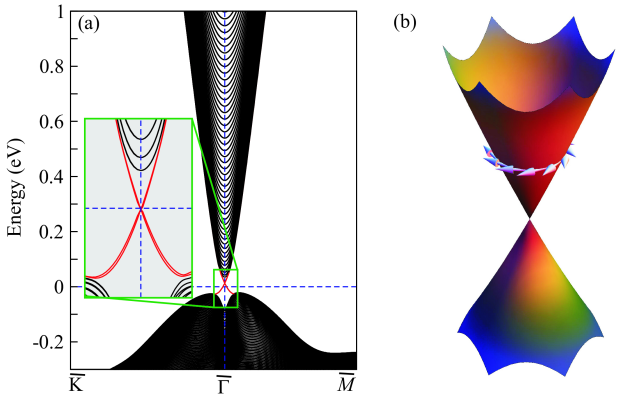

FIG. 3. (color online) TB energy band structures of the (a) (001) surface and (b) corresponding left-handed spin texture around the Fermi energy for NaBaBi. Inset shows Dirac points resembling local energy dispersion around the Fermi energy at the Γ points. The surface projected momenta are indicated in Fig. 1(b). Fermi energy is set to zero.

The TI phase is further confirmed by the direct surface state calculations. Considering that band inversion occurs between the Na s and Bi p states near the Fermi energy, the MLWFs are derived from the atomic-like Na s and Bi p orbitals to obtain the TB parameters. Then we construct the Hamiltonians of a slab for the (001) surface with a thickness of 200 unit cells and obtain the surface band structure from direct diagonalization. As shown in Fig. 3, the surface exhibits nontrivial Dirac-cone-type TSSs inside the bulk band gap. Because of the absence of inversion symmetry, the two Dirac cones on the top and bottom surfaces of the slab are not degenerate in energy, especially when they extend far from the Brillouin zone (BZ) center. As in most TIs, the surface Dirac cone of NaBaBi exhibits left-handed spin texture in the upper Dirac cone [Fig. 3(b)]. These results unambiguously demonstrate the topologically nontrivial features of NaBaBi.

As observed in the bulk band structure, the Ba $5d$ state appears as the second-lowest conduction band above the Na s state. Next, we show that the compressive pressure can shift the Ba d band down to realize an inversion of the Ba d and Bi p bands, i.e., a new TI phase. At the

same time, the Na s state is pushed up into the conduction bands, and the original Na s and Bi p inversion is removed. In the crystal field of the $BaBi_6$ octahedron [Fig. 1(c)], the low-energy t_{2g} bands are further split by strong distortion of the octahedron, where Ba d_{z^2} becomes the lowest band of the t_{2g} states (the z direction corresponds to the crystal c axis). Under compressive pressure that shrinks the $BaBi_6$ octahedron, the crystal field splitting of the Ba d states increases, so the lowest band, Ba d_{z^2}, is pushed down in energy. In the crystal field of the $NaBi_4$ tetrahedron [Fig. 1(d)], compressive pressure will simply increase the energy of the Na s state by enhancing the Coulomb repulsion of Bi^{3-} anions.

In the calculations, we apply the external pressure in two different ways: as hydrostatic pressure and as uniaxial pressure. Under hydrostatic pressure, we first estimate the bulk modulus by fitting the total energy dependence on the volume with Murnaghan's equation [28] and obtained $B_0 = 25$ GPa, which awaits validation by future experiments. Under uniaxial pressure, a tensile strain is applied along the c axis while the a and b axes are optimized, which is equivalent to applying in-plane compressive strain in the ab plane, such as that induced by a substrate. Under both types of pressure, the Ba d_{z^2} band shifts down and the Na s band shifts up, as expected. As a consequence, two topological phase transitions occur with increasing pressure. During the first transition, at a hydrostatic pressure of 1.5 GPa (uniaxial pressure of 2 GPa), because of the upshift of the Na s state, the band inversion between Na s and Bi p disappears. Thus, NaBaBi changes from a TI into a normal insulator. During the second transition, at a hydrostatic pressure of 7 GPa (uniaxial pressure of 12 GPa), because of the downshift of the Ba d_{xy} state, a new inversion occurs between Ba d and Bi p at the Γ point. Therefore, NaBaBi changes from a normal insulator to a TI phase. We show the phase diagram with respect to the pressure in Fig. 4, where two TI phases, nontrivial-I and nontrivial-II, are separated by a trivial insulator phase.

As an example, we perform a detailed analysis of the electronic structures at a hydrostatic pressure of 10 GPa. The nontrivial-II phase at other pressures (hydrostatic and uniaxial) exhibit the same band order and just different band gaps. The DFT band structures without and with SOC are compared in Figs. 5(a) and (b). Before SOC is included, the Na s state is pushed up as the second-lowest conduction band compared to the case without pressure, and Ba d_z^2 becomes the lowest conduction band. Then SOC induces band inversion between the Ba d_z^2 and Bi p_z states. The evolution of the NaBaBi band structures is further illustrated with respect to SOC and pressure. To demonstrate the topological feature, we also calculate the surface state on the (001) surface using a slab model. The MLWFs here are derived from the Na s, Bi p, and Ba d atomic-like orbitals. The corresponding surface band structure is shown in Fig. 6(a). We can clearly see the Dirac-cone-type TSSs inside the bulk band gap. Unlike the previous TI phase with s-p inversion, however, this p-d-inverted TI phase exhibits right-handed spin texture for the upper Dirac cone on the top surface, as shown in Fig. 6(b). Therefore, we obtain different spin textures in a single material, NaBaBi, via band structure engineering.

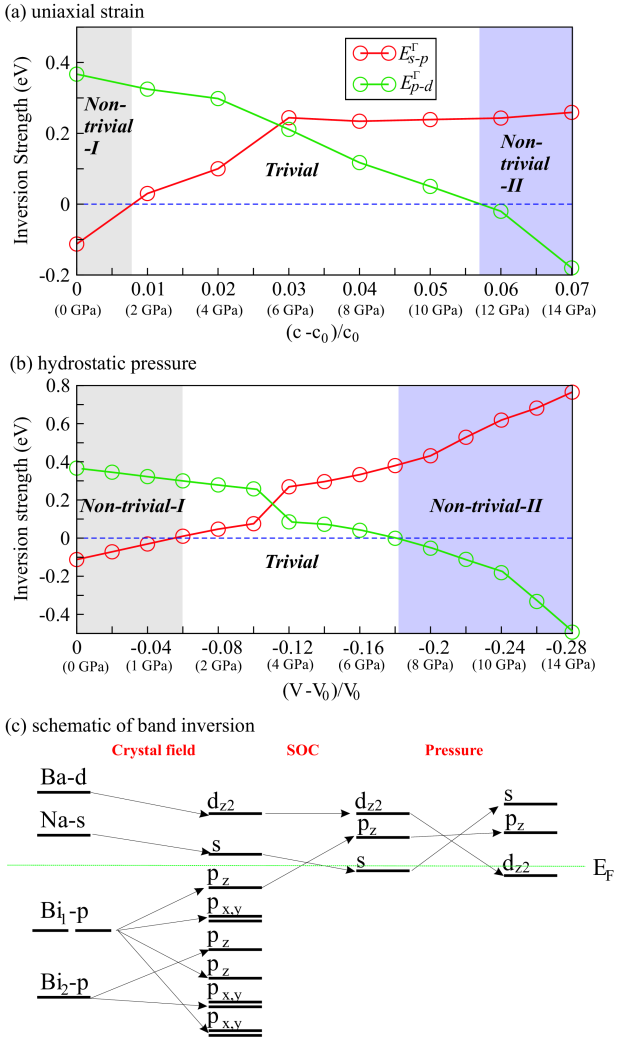

FIG. 4. (color online) Evolution of band inversion strengths of $E^{\Gamma}_{s-p} = E^{\Gamma}_{Na-s} - E^{\Gamma}_{Bi-p_z}$ and $E^{\Gamma}_{d-p} = E^{\Gamma}_{Ba-d_{z^2}} - E^{\Gamma}_{Bi-p_z}$ under (a) uniaxial strain in c direction and (b) hydrostatic pressure. Negative values of the inversion strength represent inverted band gaps, i.e., the TI phase. V_0 and c_0 are the volume and lattice constant in the equilibrium state, respectively, whereas V and c are those under the pressure or strain state. The two shaded areas in both top and bottom panels are topologically nontrivial states with p-d (nontrivial-II) and s-p band inversion (nontrivial-I), and the bright blocks are topologically trivial states.

To understand the origin of the different spin textures in NaBaBi, we also construct the effective Hamiltonian of this system using the invariant theory.[29] We focus on the low-energy physics around the Γ point, at which the wavevector group is D_{3h}. Because the spin

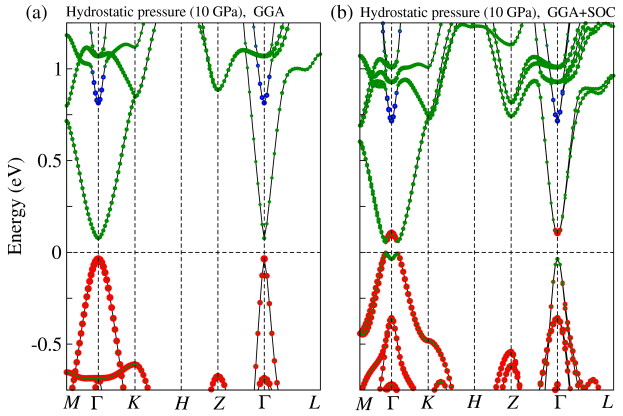

FIG. 5. (color online) Bulk band structures for NaBaBi (a) without and (b) with SOC under a hydrostatic pressure of 10 GPa. Sizes of blue, red, and green dots represent the weight contributions of Na s, Bi p, and Ba d orbitals, respectively. High-symmetry momenta are implied in Fig. 1(b), and the Fermi energy has been tuned to zero. Original s-p inversion changes to p-d inversion.

is taken into account, we need to consider the double group of D_{3h}, which possesses only three 2D irreducible representations (irreps), denoted as $\bar{\Gamma}_{7,8,9}$, which are defined in Appendix A. It turns out that both the s orbital of Na atoms and the d_{z^2} orbital of Ba atoms belong to the $\bar{\Gamma}_7$ irrep, whereas the p orbital of Bi atoms corresponds to the $\bar{\Gamma}_8$ irrep. This suggests that both the s-p inversion and p-d inversion can be described by the same effective Hamiltonian. Under the basis $|\bar{\Gamma}_7, 1/2\rangle, |\bar{\Gamma}_7, -1/2\rangle, |\bar{\Gamma}_8, 1/2\rangle, |\bar{\Gamma}_8, -1/2\rangle$, where the $\bar{\Gamma}_7$ band is for the s or d orbital and the $\bar{\Gamma}_8$ band is for the p orbital, the effective Hamiltonian can be written as $H_\alpha = \epsilon(\mathbf{k})I_{4\times4} + M(\mathbf{k})\Gamma_5 + P_\alpha k_z \Gamma_{45} + Q_\alpha(k_x\Gamma_{25} - k_y\Gamma_{15})$, where $\epsilon_\alpha(\mathbf{k}) = \epsilon_{\alpha,0} + \epsilon_{\alpha,1}k_{||}^2 + \epsilon_{\alpha,2}k_z^2$, and $M_\alpha(\mathbf{k}) = M_{\alpha,0} + M_{\alpha,1}k_{||}^2 + M_{\alpha,2}k_z^2$. Here $\alpha = s$ or d when the $\bar{\Gamma}_7$ states are given by the s or d orbitals, respectively. Γ_i and Γ_{ij} are Γ matrices, and ϵ, M, P, and Q are material-dependent parameters. The details of the construction of the model are given in Appendix A.

For comparison with the *ab initio* calculations, we choose an open boundary condition along the z direction and calculate the surface states and the corresponding spin texture on a finite slab using the above effective Hamiltonian. We find that the spin texture is right-handed for $\frac{P_\alpha}{Q_\alpha} < 0$ and left-handed for $\frac{P_\alpha}{Q_\alpha} > 0$, which is shown in detail in the appendices. A comparison of this with the *ab initio* calculations suggests $\frac{P_s}{Q_s} > 0$ for s-p inversion and $\frac{P_d}{Q_d} < 0$ for p-d inversion. The parameters P_α and Q_α are related to microscopic wave functions at the Γ point. $P_\alpha = -a\frac{\hbar}{m}\langle\alpha|\partial_z|p_z\rangle$, and $Q_\alpha = -b\frac{\hbar}{m}\langle\alpha|\partial_x|p_x\rangle$, where a and b are coefficients for the coupling between $|p_z, \sigma\rangle$ and $|p_\pm, \sigma\rangle$ of the p orbitals due to SOC, as shown in Appendix B. The different crystal environments for the s orbitals in Na atoms and the d orbitals in Ba atoms should be responsible for the opposite signs of $\frac{P_s}{Q_s}$ and $\frac{P_d}{Q_d}$. In the appendices, we also discuss the relationship between the spin texture and mirror Chern number for the s-p and p-d inversions. This relationship is similar to that for the opposite spin textures in HgTe and HgS.[11]

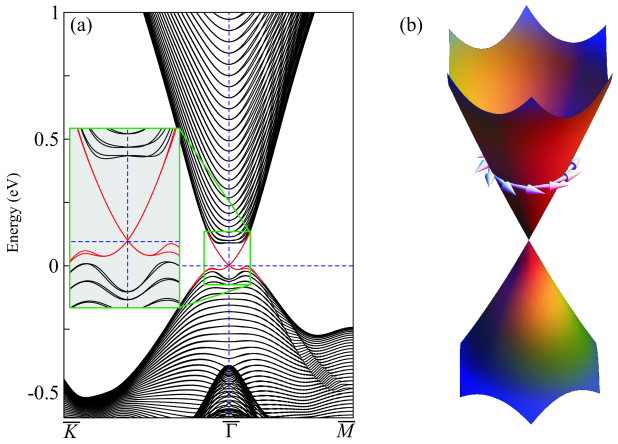

FIG. 6. (color online) (a) TB surface band structure on (001) surface with p-d band inversion under hydrostatic pressure of 10 GPa. Inset shows local bands around Fermi energy at Γ point. (b) Corresponding surface spin helical Dirac cone. Original left-handed spin texture in p-s inversion phase changes to right-handed.

IV. SUMMARY

In conclusion, inspired by the 3D topological Dirac semimetal Na_3Bi, we theoretically propose another topologically nontrivial state in NaBaBi. Two distinct TI states with different surface spin textures are achieved via band engineering. The native TI phase, with s-p band inversion, exhibits left-handed spin texture in the Dirac-type surface states. Under external pressure, the other nontrivial state, which has p-d inversion and exhibits right-handed helical spin texture, can be induced. This is further explained by the effective Hamiltonians constructed, in which s-p and p-d inverted TI phases exhibit opposite mirror Chern numbers and thus opposite spin helicity. Because the d orbitals participate in the band inversion, it is possible to bring the correlation effect into the TI phase in this compound.

ACKNOWLEDGMENTS

Thanks to S. Yunoki and the RIKEN Integrated Cluster of Clusters (RICC) for computational resources. B.Y. and C.F. acknowledge funding support by the ARCHES award from the Federal German Ministry for Education and Research (BMBF) and the ERC Advanced Grant (291472), respectively.

Appendix A: Construction of effective Hamiltonian by symmetry

In this section, we will show how to construct the effective Hamiltonian on the basis of the crystal symmetry. The point group at the Γ point in momentum space for NaBaBi is D_{3h}. The character table for the D_{3h} double group is shown in Table I. To distinguish the Γ matrices that we will use later, we use $\bar{\Gamma}$ to denote different irreducible representations (irreps). Only double irreps can be used to describe electron systems with spin. Thus, we consider only the $\bar{\Gamma}_{7,8,9}$ irreps. The basis functions for the $\bar{\Gamma}_{7,8,9}$ irreps are denoted as $|\bar{\Gamma}_7\rangle = |j = 1/2, m_j = \pm 1/2\rangle$, $|\bar{\Gamma}_8\rangle = z|j = 1/2, m_j = \pm 1/2\rangle$, and $|\bar{\Gamma}_9\rangle = |j = 3/2, m_j = \pm 3/2\rangle$, respectively.

TABLE I. Character table for the double group of D_{3h}.

D_{3h}	E	$\bar{E}$	$\sigma_h\&\bar{\sigma}_h$	$2C_3$	$2\bar{C}_3$	$2S_3$	$2\bar{S}_3$	$3C_2'\&3\bar{C}_2'$	$3\sigma_v\&3\bar{\sigma}_v$
$\bar{\Gamma}_1$	1	1	1	1	1	1	1	1	1
$\bar{\Gamma}_2$	1	1	1	1	1	1	1	-1	-1
$\bar{\Gamma}_3$	1	1	-1	1	1	-1	-1	1	-1
$\bar{\Gamma}_4$	1	1	-1	1	1	-1	-1	-1	1
$\bar{\Gamma}_5$	2	2	-2	-1	-1	1	1	0	0
$\bar{\Gamma}_6$	2	2	2	-1	-1	-1	-1	0	0
$\bar{\Gamma}_7$	2	-2	0	1	-1	$\sqrt{3}$	$-\sqrt{3}$	0	0
$\bar{\Gamma}_8$	2	-2	0	1	-1	$-\sqrt{3}$	$\sqrt{3}$	0	0
$\bar{\Gamma}_9$	2	-2	0	-2	2	0	0	0	0

The orbitals of NaBaBi near the Fermi energy are s orbital of Na atoms, p orbital of Bi atoms, and d orbital of Ba atoms. From a first-principle calculation, we find that the main component of the p (d) orbital of Bi (Ba) atoms is p_z (d_{z^2}) orbital. Next, we will determine the irreps to which the s, p_z, and d_{z^2} orbitals belong.

To distinguish irreps $\bar{\Gamma}_{7,8,9}$, we need to consider only the characters under C_3 and S_3 operations. $C_3|s(d_{z^2}, p_z), \uparrow\rangle = e^{-i\pi/3}|s(d_{z^2}, p_z), \uparrow\rangle$. $C_3|s(d_{z^2}, p_z), \downarrow\rangle = e^{i\pi/3}|s(d_{z^2}, p_z), \downarrow\rangle$. All the characters under C_3 rotation for the s, p_z, and d_{z^2} orbitals are $\chi = e^{-i\pi/3} + e^{i\pi/3} = 1$.

For the S_3 operation, $S_3|s(d_{z^2}), \uparrow\rangle = ie^{-i\pi/3}|s(d_{z^2}), \uparrow\rangle$, and $S_3|s(d_{z^2}), \downarrow\rangle = -ie^{i\pi/3}|s(d_{z^2}), \downarrow\rangle$. The character is $\chi = ie^{-i\pi/3} - ie^{i\pi/3} = \sqrt{3}$. Thus, both the s and d_{z^2} orbitals belong to irrep $\bar{\Gamma}_7$. For the p_z orbital, however, $S_3|p_z, \uparrow\rangle = -ie^{-i\pi/3}|p_z, \uparrow\rangle$, and $S_3|p_z, \downarrow\rangle = ie^{i\pi/3}|p_z, \downarrow\rangle$. The character is $\chi = -ie^{-i\pi/3} + ie^{i\pi/3} = -\sqrt{3}$. Thus, the p_z orbital belongs to irrep $\bar{\Gamma}_8$.

As shown in Table II, the s and d_{z^2} orbitals belong to irrep $\bar{\Gamma}_7$, whereas the p_z orbital belongs to irrep $\bar{\Gamma}_8$.

After identifying the irreps for each orbital near the Fermi energy, we use the representation theory to construct the effective model for NaBaBi near the Γ point in momentum space. Basically, we follow the procedure in Ref. 30.

The effective Hamiltonian we will construct has the following basis: $\xi = (|\bar{\Gamma}_7, 1/2\rangle, |\bar{\Gamma}_7, -1/2\rangle, |\bar{\Gamma}_8, 1/2\rangle, |\bar{\Gamma}_8, -1/2\rangle)^T$. The

TABLE II. Character table for s, p_z, and d_{z^2} orbitals with spin.

Orbitals with spin	$2C_3$	$2S_3$	Irreps
$s\uparrow$, $s\downarrow$	1	$\sqrt{3}$	$\bar{\Gamma}_7$
$p_z\uparrow$, $p_z\downarrow$	1	$-\sqrt{3}$	$\bar{\Gamma}_8$
$d_{z^2}\uparrow$, $d_{z^2}\downarrow$	1	$\sqrt{3}$	$\bar{\Gamma}_7$

transformation matrices of the symmetry operations in D_{3h} group under this basis are

- Time reversal operation: $T = diag[-i\sigma_2 K, -i\sigma_2 K] = -\tau_3 \otimes i\sigma_2 K$;
- Mirror operation along the z direction: $\mathcal{M}_z = diag[i\sigma_3, -i\sigma_3] = \tau_3 \otimes i\sigma_3$;
- C_3 operation: $C_3 = diag[e^{-i\frac{\pi}{3}}, e^{i\frac{\pi}{3}}, e^{-i\frac{\pi}{3}}, e^{i\frac{\pi}{3}}]$;
- $C_{2,x}$ operation along the x direction: $C_{2,x} = diag[-i\sigma_1, i\sigma_1] = -\tau_3 \otimes i\sigma_1$;
- Mirror operation along the y direction: $\mathcal{M}_y = diag[i\sigma_2, i\sigma_2] = \tau_0 \otimes i\sigma_2$,

where σ_i and τ_i are the Pauli matrices in spin and band space, respectively. Here we select a particular gauge such that $T = i\sigma_2 K$ in spin-up and spin-down space, where K represents complex conjugation. We set $|\bar{\Gamma}_7, \pm 1/2\rangle = i|s(d_{z^2}), \uparrow(\downarrow)\rangle$ to obtain $T = -\tau_3 \otimes i\sigma_2 K$. By using this convention, we make all the parameters real in the Hamiltonian that we will derive.

We start with 5 Dirac Γ matrices on the basis mentioned above, which are defined as

$$\Gamma_1 = \tau_1 \otimes \sigma_1, \quad \Gamma_2 = \tau_1 \otimes \sigma_2, \quad \Gamma_3 = \tau_1 \otimes \sigma_3, \quad \Gamma_4 = \tau_2 \otimes 1, \quad \Gamma_5 = \tau_3 \otimes 1. \tag{A1}$$

They satisfy Clifford algebra: $\{\Gamma_a, \Gamma_b\} = 2\delta_{ab}$. The other 10 Γ matrices are constructed by $\Gamma_{ab} = [\Gamma_a, \Gamma_b]/2i$ and are expressed explicitly as

$$\Gamma_{ij} = [\tau_1 \otimes \sigma_i, \tau_1 \otimes \sigma_j]/2i = 1 \otimes \varepsilon_{ijk}\sigma_k, \tag{A2}$$
$$\Gamma_{i4} = [\tau_1 \otimes \sigma_i, \tau_2 \otimes 1]/2i = \tau_3 \otimes \sigma_i, \tag{A3}$$
$$\Gamma_{i5} = [\tau_1 \otimes \sigma_i, \tau_3 \otimes 1]/2i = -\tau_2 \otimes \sigma_i, \tag{A4}$$
$$\Gamma_{45} = [\tau_2 \otimes 1, \tau_3 \otimes 1]/2i = \tau_1 \otimes 1, \tag{A5}$$

where $i, j = 1, 2, 3$.

Under the time-reversal transformation matrix, the Γ matrices satisfy

$$T\Gamma_i T^{-1} = \Gamma_i, \quad i = 1, 2, 3, 4, 5; \tag{A6}$$
$$T\Gamma_{ij} T^{-1} = -\Gamma_{ij}, \quad i, j = 1, 2, 3, \quad i \neq j; \tag{A7}$$
$$T\Gamma_{i4} T^{-1} = -\Gamma_{i4}, \quad i = 1, 2, 3; \tag{A8}$$
$$T\Gamma_{i5} T^{-1} = -\Gamma_{i5}, \quad i = 1, 2, 3; \tag{A9}$$
$$T\Gamma_{45} T^{-1} = -\Gamma_{45}. \tag{A10}$$

Using the $\mathcal{M}_z$, $C_{2,x}$, and $\mathcal{M}_y$ transformation matrices, we have

$$\mathcal{M}_z : \mathcal{M}_z\Gamma_{1,2,5,12,34,15,25}\mathcal{M}_z^{-1} = \Gamma_{1,2,5,12,34,15,25},$$
$$\mathcal{M}_z\Gamma_{3,4,23,31,14,24,35,45}\mathcal{M}_z^{-1} = -\Gamma_{3,4,23,31,14,24,35,45}, \quad \text{(A11)}$$
$$C_{2,x} : C_{2,x}\Gamma_{2,3,5,23,14,25,35}C_{2,x}^{-1} = \Gamma_{2,3,5,23,14,25,35},$$
$$C_{2,x}\Gamma_{1,4,31,12,24,34,15,45}C_{2,x}^{-1} = -\Gamma_{1,4,31,12,24,34,15,45}, \quad \text{(A12)}$$
$$\mathcal{M}_y : \mathcal{M}_y\Gamma_{2,4,5,31,24,25,45}\mathcal{M}_y^{-1} = \Gamma_{2,4,5,31,24,25,45},$$
$$\mathcal{M}_y\Gamma_{1,3,12,23,14,34,15,35}\mathcal{M}_y^{-1} = -\Gamma_{1,3,12,23,14,34,15,35}. \quad \text{(A13)}$$

Under C_3 rotation symmetry, the Γ matrices satisfy $\Gamma'_\theta = e^{i\Sigma/2\theta}\Gamma e^{-i\Sigma/2\theta}$, with $\Sigma = 1 \otimes \sigma_z$. Furthermore, $\frac{d\Gamma'_\theta}{d\theta} = \frac{i}{2}[\Sigma, \Gamma'_\theta]$. Thus, the commutation relations between Σ and Γ are important here, and are listed as follows:

$$[\Sigma, \Gamma_1] = 2i\Gamma_2, \qquad [\Sigma, \Gamma_2] = -2i\Gamma_1, \quad \text{(A14)}$$
$$[\Sigma, \Gamma_3] = [\Sigma, \Gamma_4] = [\Sigma, \Gamma_5] = 0, \quad \text{(A15)}$$
$$[\Sigma, \Gamma_{12}] = 0, \qquad [\Sigma, \Gamma_{34}] = 0, \quad \text{(A16)}$$
$$[\Sigma, \Gamma_{31}] = -2i\Gamma_{23}, \qquad [\Sigma, \Gamma_{23}] = 2i\Gamma_{31}, \quad \text{(A17)}$$
$$[\Sigma, \Gamma_{14}] = 2i\Gamma_{24}, \qquad [\Sigma, \Gamma_{24}] = -2i\Gamma_{14}, \quad \text{(A18)}$$
$$[\Sigma, \Gamma_{15}] = 2i\Gamma_{25}, \qquad [\Sigma, \Gamma_{25}] = -2i\Gamma_{15}, \quad \text{(A19)}$$
$$[\Sigma, \Gamma_{35}] = 0, \qquad [\Sigma, \Gamma_{45}] = 0. \quad \text{(A20)}$$

Using these commutation relations, we can easily solve for Γ'_θ, which are expressed as

$$\Gamma'_1(\theta) = \Gamma_1\cos\theta + \Gamma_2\sin\theta,$$
$$\Gamma'_2(\theta) = \Gamma_1\sin\theta - \Gamma_2\cos\theta, \quad \text{(A21)}$$
$$\Gamma'_{23}(\theta) = \Gamma_{23}\cos\theta + \Gamma_{31}\sin\theta,$$
$$\Gamma'_{31}(\theta) = \Gamma_{31}\cos\theta - \Gamma_{23}\sin\theta, \quad \text{(A22)}$$
$$\Gamma'_{14}(\theta) = \Gamma_{14}\cos\theta + \Gamma_{24}\sin\theta,$$
$$\Gamma'_{24}(\theta) = \Gamma_{14}\sin\theta - \Gamma_{24}\cos\theta, \quad \text{(A23)}$$
$$\Gamma'_{15}(\theta) = \Gamma_{15}\cos\theta + \Gamma_{25}\sin\theta,$$
$$\Gamma'_{25}(\theta) = \Gamma_{15}\sin\theta - \Gamma_{25}\cos\theta, \quad \text{(A24)}$$
$$\Gamma'_3(\theta) = \Gamma_3, \qquad \Gamma'_4(\theta) = \Gamma_4,$$
$$\Gamma'_5(\theta) = \Gamma_5, \qquad \Gamma'_{34} = \Gamma_{34}, \qquad \Gamma'_{12} = \Gamma_{12},$$
$$\Gamma'_{35} = \Gamma_{35}, \qquad \Gamma'_{45} = \Gamma_{45}. \quad \text{(A25)}$$

Γ matrix pairs $[\Gamma_1, \Gamma_2]$, $[\Gamma_{23}, \Gamma_{31}]$, $[\Gamma_{14}, \Gamma_{24}]$, and $[\Gamma_{15}, \Gamma_{25}]$ transform as the x,y components of a vector under C_3 rotation. The other seven Γ matrices transform as scalars or pseudo-scalars under C_3 rotation.

Because $\bar{\Gamma}_7 \otimes \bar{\Gamma}_8 = \bar{\Gamma}_3 \oplus \bar{\Gamma}_4 \oplus \bar{\Gamma}_5$, here we consider only irreps $\bar{\Gamma}_3$, $\bar{\Gamma}_4$, and $\bar{\Gamma}_5$ for the effective model. The character table for these three irreps is given in Table III.

Under C_3 rotation, we have two rotationally invariant combinations of Γ matrices and $\mathbf{k}$ that preserve time-reversal symmetry. They are $k'_x\Gamma'_{25} - k'_y\Gamma'_{15} = k_x\Gamma_{25} - k_y\Gamma_{15}$ and $k'_x\Gamma'_{15} + k'_y\Gamma'_{25} = k_x\Gamma_{15} + k_y\Gamma_{25}$. However, under the $\mathcal{M}_y$ operation, $\mathcal{M}_y\Gamma'_{15}\mathcal{M}_y^{-1} = -\Gamma'_{15}$, and $\mathcal{M}_y\Gamma'_{25}\mathcal{M}_y^{-1} = +\Gamma'_{25}$; $\mathcal{M}_y k_x = k_x$, and $\mathcal{M}_y k_y = -k_y$. The effective Hamiltonian needs to preserve the mirror symmetry $\mathcal{M}_y$ and time-reversal symmetry simultaneously. Therefore, the qualified term reads $k_x\Gamma_{25} - k_y\Gamma_{15}$.

TABLE III. Character table of Γ matrices and polynomials of the momentum $\mathbf{k}$.

Representation	Basis functions	T
$\bar{\Gamma}_3$	Γ_3	+
	Γ_{35}	-
$\bar{\Gamma}_4$	k_z	-
	Γ_4	+
	Γ_{45}	-
$\bar{\Gamma}_5$	(k_x, k_y)	-
	$(k_x^2 - k_y^2, k_x k_y)$	+
	(Γ_1, Γ_2)	+
	$(\Gamma_{15}, \Gamma_{25})$	-

Similarly, we obtain another term, $2k_xk_y\Gamma_1 + (k_x^2 - k_y^2)\Gamma_2$. Thus, the effective Hamiltonian on the new basis, $\xi = (|\bar{\Gamma}_7, 1/2\rangle, |\bar{\Gamma}_7, -1/2\rangle, |\bar{\Gamma}_8, 1/2\rangle, |\bar{\Gamma}_8, -1/2\rangle)^T$, up to the second order of $\mathbf{k}$, is expressed as $H = \epsilon(\mathbf{k})I_{4\times4} + M(\mathbf{k})\Gamma_5 + Pk_z\Gamma_{45} + Q(k_x\Gamma_{25} - k_y\Gamma_{15}) + Q'(2k_xk_y\Gamma_1 + (k_x^2 - k_y^2)\Gamma_2)$. Explicitly, the effective Hamiltonian can be written as

$$H_{eff} = \begin{pmatrix} M_7(\mathbf{k}) & 0 & Pk_z & Qk_- + Q'(2k_xk_y - i(k_x^2 - k_y^2)) \\ & M_7(\mathbf{k}) & -Qk_+ + Q'(2k_xk_y + i(k_x^2 - k_y^2)) & Pk_z \\ & h.c. & M_8(\mathbf{k}) & 0 \\ & & & M_8(\mathbf{k}) \end{pmatrix}, \quad \text{(A26)}$$

where

$$\epsilon(\mathbf{k}) = \epsilon_0 + \epsilon_1 k_{||}^2 + \epsilon_2 k_z^2,$$
$$M(\mathbf{k}) = M_0 + M_1 k_{||}^2 + M_2 k_z^2,$$
$$M_7(\mathbf{k}) = \epsilon(\mathbf{k}) + M(\mathbf{k}),$$
$$M_8(\mathbf{k}) = \epsilon(\mathbf{k}) - M(\mathbf{k}), \quad \text{(A27)}$$

and ϵ_i, M_i, P, P', and Q are real. Because $\epsilon(\mathbf{k})$,

$M(\mathbf{k})$, $I_{4\times4}$, and Γ_5 belong to the $\bar{\Gamma}_1$ irrep and they are all even under time-reversal symmetry, combinations of these terms, $\epsilon(\mathbf{k})I_{4\times4}$ and $M(\mathbf{k})\Gamma_5$, are invariant under all the operations of the D_{3h} point group. Thus, we also need to include them in the effective Hamiltonian. This Hamiltonian is used to explain the spin textures for both the *s-p* and *d-p* inversions in NaBaBi.

Appendix B: Spin helicity and mirror Chern number

We consider a slab described by the effective Hamiltonian in Eq. (A26) with the open boundary along the k_z direction. The spin texture is calculated numerically with appropriate parameters for qualitative agreement with the result obtained by the first-principle methods. The parameters are listed in Table IV. In Fig. 7, we show the Fermi arc and spin texture on the upper Dirac cone of the top surface of NaBaBi on the k_xk_y plane. The Fermi arc is a circle, and the directions of the spins are tangential to the circle. The spin texture is right-handed (left-handed) for NaBaBi with *d-p* inversion (*s-p* inversion), which is consistent with the results of the first-principle calculations. The key point for the opposite spin textures is found to be the sign of P/Q. For $P/Q > 0$, the spin texture is left-handed, whereas for $P/Q < 0$, it is right-handed.

TABLE IV. Parameters for NaBaBi. For *s-p* inversion, $\epsilon_1 = 0.05$ eV $\cdot$ Å, $Q = 0.5$ eV $\cdot$ Å, and $Q' = -0.2$ eV $\cdot$ Å^2; for *d-p* inversion, $\epsilon_1 = -0.05$ eV $\cdot$ Å, $Q = -0.5$ eV $\cdot$ Å, and $Q' = 0.2$ eV $\cdot$ Å^2.

ϵ_0[eV]	ϵ_1[eV $\cdot$ Å^2]	ϵ_2[eV $\cdot$ Å^2]	M_0[eV]	M_1[eV $\cdot$ Å^2]	M_2[eV $\cdot$ Å^2]	P[eV $\cdot$ Å]	Q[eV $\cdot$ Å]	Q'[eV $\cdot$ Å^2]
0	$\pm$ 0.05	0	-0.5	5	5	1	$\pm$ 0.5	$\pm$ 0.2

This can be understand from the mirror symmetry along the y direction. Next, we hope to unveil the physics behind the relationship between P/Q and the spin texture. Because the system preserves mirror symmetry with respect to the $k_y = 0$ plane, the Hamiltonian commutes with the mirror operator $\mathcal{M}_y$: $\mathcal{M}_y H(k_x, 0, k_z)\mathcal{M}_y^{-1} = H(k_x, 0, k_z)$. Therefore, the Hamiltonian and the mirror operator can be diagonalized simultaneously. The mirror operator along the y direction is given by $\mathcal{M}_y = \tau_0 \otimes i\sigma_2$. In the $+i$ mirror parity subspace, the common eigen-wavefunctions are $\Psi(+i)_1 = \frac{1}{\sqrt{2}}(1, i, 0, 0)^T$ and $\Psi(+i)_2 = \frac{1}{\sqrt{2}}(0, 0, 1, i)^T$. On these two basis functions, the projected Hamiltonian reads

$$H_{+i} = \begin{pmatrix} M_7 & P(k_z + i\frac{Q}{P}k_x) + Q'k_x^2 \\ P(k_z - i\frac{Q}{P}k_x) + Q'k_x^2 & M_8 \end{pmatrix} \tag{B1}$$

,

where $M_7(\mathbf{k}) = \epsilon(\mathbf{k}) + M(\mathbf{k})$, and $M_8(\mathbf{k}) = \epsilon(\mathbf{k}) - M(\mathbf{k})$. Q' is much smaller than P and Q and is neglected in the analysis below.

The Hamiltonian in the $+i$ mirror parity subspace has a nonzero Chern number, which can be calculated from $n = \int_{BZ} \frac{d^2k}{4\pi}\hat{\mathbf{d}} \cdot (\frac{\partial\hat{\mathbf{d}}}{\partial k_z} \times \frac{\partial\hat{\mathbf{d}}}{\partial k_x})$, where $\hat{\mathbf{d}} = \frac{1}{|\mathbf{d}|}(d_x, d_y, d_z)$ when we write H_{+i} as $H_{+i} = \epsilon(\mathbf{k}) + \mathbf{d} \cdot \sigma$.[31] Because the Chern number n_{-i} for the effective Hamiltonian in the $-i$ mirror parity subspace always takes the opposite value because of time-reversal symmetry, $n_{-i} = -n_{+i}$, the total Chern number is zero, and only the mirror Chern number, defined as $n_M \equiv \frac{n_{+i} - n_{-i}}{2} = {n_{+i}}^{32}$, can be nonzero. For $P/Q > 0$, $n_M = -1$, whereas for $P/Q < 0$, $n_M = 1$. The mirror Chern number is directly related to the spin texture of the surface states according to the bulk–edge correspondence. Now let us consider that the open boundary along the z direction and the mirror symmetry along the y direction still exist for $k_y = 0$. For the $+i$ mirror parity subspace and $n_{+i} = 1$, there is a chiral edge mode with positive velocity along the k_x direction. Because the mirror parity $+i$ subspace corresponds to spin up along the y direction, this chiral mode should have spin up along the y direction. The spin-down state along the y direction is in the $-i$ mirror parity subspace and thus possesses negative velocity.[11] Therefore, the entire system has a right-handed spin texture for $P/Q < 0$. When $P/Q > 0$, the mirror Chern number is -1, and the spin texture is left-handed.

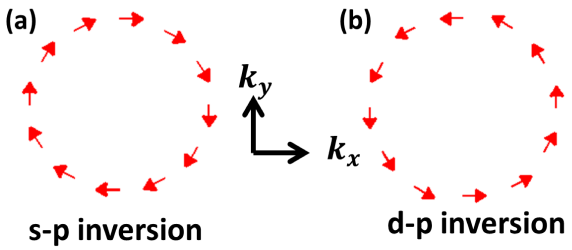

FIG. 7. (Color online). Spin textures on the Fermi arc with energy $E_F = 0.1$ eV (compared with the Dirac point energy) on the upper Dirac cone of the top surface of NaBaBi. Panels (a) and (b) correspond to s-p and d-p inversion in NaBaBi, which have left-handed and right-handed spin textures, respectively, on the upper Dirac cone of the top surface of NaBaBi.

Next, we will explain what determines the opposite signs of P/Q for s-p and d-p inversion. Without losing generality, we neglect the off-diagonal quadratic term for simplicity. We can write the basis functions for irreps $\bar{\Gamma}_7$ and $\bar{\Gamma}_8$ in terms of the s, p_z, and d_{z^2} orbitals. In the $+i$ mirror parity subspace, there are two ways to express the basis functions for irrep $\bar{\Gamma}_7$, $\frac{1}{\sqrt{2}}(|\bar{\Gamma}_7, 1/2\rangle_z + i|\bar{\Gamma}_7, -1/2\rangle_z)$, which are $\Psi(s)_{+i} = i\frac{1}{\sqrt{2}}(|s,\uparrow_z\rangle + i|s,\downarrow_z\rangle)$ and $\Psi(d_{z^2})_{+i} = i\frac{1}{\sqrt{2}}(|d_{z^2},\uparrow_z\rangle + i|d_{z^2},\downarrow_z\rangle)$, where the spins are along the z direction. The basis function for irrep $\bar{\Gamma}_8$ in the mirror parity $\lambda = +i$ subspace is $\Psi(p_z)_{+i} = \frac{1}{\sqrt{2}}(|\bar{\Gamma}_8, 1/2\rangle_z + i|\bar{\Gamma}_8, 1/2\rangle_z)$.

Because of SOC, $|p_z,\uparrow_z\rangle$ can be mixed with the $|(p_x + ip_y),\downarrow_z\rangle$ state. Similarly, the $|p_z,\downarrow_z\rangle$ state can be mixed with the $|(p_x - ip_y),\uparrow_z\rangle$ state. The basis functions for $\bar{\Gamma}_8$ irrep, written in terms of the p orbitals, read

$$|\bar{\Gamma}_8, 1/2\rangle_z = a|p_z,\uparrow_z\rangle - b|(p_x + ip_y),\downarrow_z\rangle,$$
$$|\bar{\Gamma}_8, -1/2\rangle_z = a|p_z,\downarrow_z\rangle + b|(p_x - ip_y),\uparrow_z\rangle, \quad \text{(B2)}$$

where $a^2 + 2b^2 = 1$. Because the main component of the p orbitals is the p_z orbital, we regard the parameter b as a perturbation. We have $a \gg b$. Here we neglect SOC between the eg and $t2g$ orbitals because of the large energy splitting between them.

To obtain the Hamiltonian in Eq. (B1), we transform the basis functions above to a set of new basis functions, where the spin quantization direction is along the y direction (the normal direction of the mirror plane). For each basis function in the mirror $\lambda = +i$ subspace, we have

$$\Psi(s)_{+i} = i|s,\uparrow_y\rangle,$$
$$\Psi(d)_{+i} = i|d_{z^2},\uparrow_y\rangle,$$
$$\Psi(p)_{+i} = \frac{1}{\sqrt{2}}(|\bar{\Gamma}_8, 1/2\rangle_z + i|\bar{\Gamma}_8, -1/2\rangle_z) = a|p_z,\uparrow_y\rangle + ib|p_x,\uparrow_y\rangle + b|p_y,\downarrow_y\rangle, \quad \text{(B3)}$$

where we have used $|\uparrow_y\rangle = \frac{1}{\sqrt{2}}(|\uparrow_z\rangle + i|\downarrow_z\rangle)$.

Thus, P and Q in Eq. (B1) can be derived in terms of a, b, and the matrix elements from $\mathbf{k}\cdot\mathbf{p}$ theory.[33] The $\mathbf{k}\cdot\mathbf{p}$ Hamiltonian reads $H_{\mathbf{k}\cdot\mathbf{p}} = \frac{\hbar}{m}\mathbf{k}\cdot\mathbf{p} = \frac{\hbar}{m}\mathbf{k}\cdot(-i\hbar\nabla) = -i\frac{\hbar^2}{m}\mathbf{k}\cdot\nabla$, where we replace $\mathbf{p}$ with $-i\hbar\nabla$ to distinguish it from the notation for the p orbitals. For s-p inversion, $P = -i\frac{\hbar^2}{m}\langle\Psi(s)_{+i}|\partial_z|\Psi(p)_{+i}\rangle = -\frac{\hbar^2}{m}a\langle s|\partial_z|p_z\rangle$, and $iQ = -i\frac{\hbar^2}{m}\langle\Psi(s)_{+i}|\partial_x|\Psi(p)_{+i}\rangle = -ib\frac{\hbar^2}{m}\langle s|\partial_x|p_x\rangle$. Recall that the s orbital is from Na atoms and the p orbitals are from Bi atoms. Similarly, for d-p inversion of NaBaBi, $P = -i\frac{\hbar^2}{m}\langle\Psi(d_{z^2})_{+i}|\partial_z|\Psi(p)_{+i}\rangle = -\frac{\hbar^2}{m}a\langle d_{z^2}|\partial_z|p_z\rangle$, and $iQ = -i\frac{\hbar^2}{m}\langle\Psi(d_{z^2})_{+i}|\partial_x|\Psi(p)_{+i}\rangle = -i\frac{\hbar^2}{m}b\langle d_{z^2}|\partial_x|p_x\rangle$.

Therefore, we have $P/Q = \frac{a\langle s|\partial_z|p_z\rangle}{b\langle s|\partial_x|p_x\rangle}$ for s-p inversion, and $P/Q = \frac{a\langle d_{z^2}|\partial_z|p_z\rangle}{b\langle d_{z^2}|\partial_x|p_x\rangle}$ for d-p inversion. This suggests that for s-p and d-p inversion, the matrix elements $\frac{\langle s|\partial_z|p_z\rangle}{\langle s|\partial_x|p_x\rangle}$ and $\frac{\langle d_{z^2}|\partial_z|p_z\rangle}{\langle d_{z^2}|\partial_x|p_x\rangle}$ have opposite signs for NaBaBi.

* Corresponding author:yan@cpfs.mpg.de

[1] M. Z. Hasan and C. L. Kane, Rev. Mod. Phys. **82**, 3045 (2010).
[2] X. L. Qi and S. C. Zhang, Rev. Mod. Phys. **83**, 1057 (2011).
[3] Haijun Zhang, Chao-Xing Liu, Xiao-Liang Qi, Xi Dai, Zhong Fang1 and Shou-Cheng Zhang, Nature Phys. **5**,438, (2009).
[4] Y. Xia, D. Qian, D. Hsieh, L.Wray, A. Pal, H. Lin, A. Bansil, D. Grauer, Y. S. Hor, R. J. Cava and M. Z. Hasan,Nature Phys. **5**, 398 (2009).
[5] D. Hsieh, Y. Xia, D. Qian, L. Wray, J. H. Dil6, F. Meier6, J. Osterwalder, L. Patthey, J. G. Checkelsky, N. P. Ong, A. V. Fedorov, H. Lin, A. Bansil, D. Grauer, Y. S. Hor, R. J. Cava and M. Z. Hasan, Nature, **460**,1101 (2009).
[6] Y. L. Chen, J. G. Analytis,J.-H. Chu, Z. K. Liu, S.-K. Mo, X. L. Qi, H. J. Zhang, D. H. Lu, X. Dai, Z. Fang, S. C. Zhang, I. R. Fisher, Z. Hussain, Z.-X. Shen, Science **325**, 178 (2009).
[7] C.-X. Liu, X.-L. Qi, H. Zhang, X. Dai, Z. Fang, and S.-C. Zhang, Phys. Rev. B **82**, 045122 (2010).

[8] Binghai Yan, Martin Jansen and Claudia Felser, Nature Phys. **9**,709 (2013).

[9] Zhijun Wang, Yan Sun, Xing-Qiu Chen, Cesare Franchini, Gang Xu, Hongming Weng, Xi Dai, and Zhong Fang, Phy. Rev. B **85**, 195320 (2012).

[10] Su-Yang Xu, Y. Xia, L. A. Wray, S. Jia, F. Meier, J. H. Dil, J. Osterwalder, B. Slomski, A. Bansil, H. Lin, R. J. Cava, M. Z. Hasan, Science, **332**, 560 (2011).

[11] Qing-Ze Wang, Shu-chun Wu, Claudia Felser, Binghai Yan, and Chao-xing Liu, arXiv preprint arXiv:1404.7091 (2014)

[12] Z. K. Liu, B. Zhou, Y. Zhang, Z. J. Wang, H. M. Weng, D. Prabhakaran, S.-K. Mo, Z. X. Shen, Z. Fang, X. Dai, Z. Hussain, and Y. L. Chen, Science 343, 864 (2014).

[13] Z. Wang, H. Weng, Q. Wu, X. Dai, and Z. Fang, Phys. Rev. B 88, 125427 (2013).

[14] Z. K. Liu, J. Jiang, B. Zhou, Z. J. Wang, Y. Zhang, H. M. Weng, D. Prabhakaran, S.-K. Mo, H. Peng, P. Dudin, T. Kim, M. Hoesch, Z. Fang, X. Dai, Z. X. Shen, D. L. Feng, Z. Hussain, and Y. L. Chen, Nature Materials 13, 677 (2014).

[15] M. Neupane, S.-Y. Xu, R. Sankar, N. Alidoust, G. Bian, C. Liu, I. Belopolski, T.-R. Chang, H.-T. Jeng, H. Lin, A. Bansil, F. Chou, and M. Z. Hasan, Nature Communications 5, (2014).

[16] S. Jeon, B. B. Zhou, A. Gyenis, B. E. Feldman, I. Kimchi, A. C. Potter, Q. D. Gibson, R. J. Cava, A. Vishwanath, and A. Yazdani, Nature Materials 13, 851 (2014).

[17] H. Yi, Z. Wang, C. Chen, Y. Shi, Y. Feng, A. Liang, Z. Xie, S. He, J. He, Y. Peng, X. Liu, Y. Liu, L. Zhao, G. Liu, X. Dong, J. Zhang, M. Nakatake, M. Arita, K. Shimada, H. Namatame, M. Taniguchi, Z. Xu, C. Chen, X. Dai, Z. Fang, and X. J. Zhou, Sci. Rep. 4, 6106 (2014).

[18] X. Wan, A. M. Turner, A. Vishwanath, and S. Y. Savrasov, Phys. Rev. B 83, 205101 (2011).

[19] Holger Hirt and Hans-Jorg Deiseroth, Z. Anorg. Allg. Chem. **630**,1357 (2004).

[20] H.-J. Zhang, S. Chadov, L. M uchler, B. Yan, X.-L. Qi, J. K ubler, S.-C. Zhang, and C. Felser, Phys. Rev. Lett. 106, 156402 (2011).

[21] B. Yan, L. Mchler, and C. Felser, Physical Review Letters 109, 116406 (2012).

[22] P. E. Bloechl, Phys. Rev. B 50, 17953 (1994).

[23] G. Kresse and J. Hafner, Phys. Rev. B **48**, 13115, (1993).

[24] G. Kresse and J. Furthmiiller, Comp. Mater. Sci. **6**, 15 (1996).

[25] J. P. Perdew, K. Burke, and M. Ernzerho, Phys. Rev. Lett. **77**, 3865 (1996)

[26] A. A. Mostofi, J. R. Yates, Y. S. Lee, I. Souza, D. Vanderbilt, and N. Marzari, Comput. Phys. Commun. **178**, 685 (2008).

[27] L. Fu and C. L. Kane, Phys. Rev. B 76, 045302 (2007).

[28] F.D. Murnaghan, Proc. Natl. Acad. Sci. U.S.A. **30**, 244 (1944).

[29] Roland Winkler, Spin-Orbit Coupling Effects in Two-Dimensional Electron and Hole Systems, Springer(2003)

[30] C.-X. Liu, X.-L. Qi, H. Zhang, X. Dai, Z. Fang, and S.-C. Zhang, Phys. Rev. B 82, 045122 (2010).

[31] X.-L. Qi, Y.-S. Wu, and S.-C. Zhang, Phys. Rev. B, 74, 085308 (2006).

[32] T. H. Hsiehthor, H. Lin, J. Liu, W. Duan, A. Bansil, and L. Fu, Nat. Commun. 3, 982 (2012).

[33] L. C. L. Y. Voon and M. Willatzen, *The kp method: electronic properties of semiconductors*, (Springer, 2009)